

Comparative analysis of ^{60}Co intensity-modulated radiation therapy*

Christopher Fox^{1,2}, H Edwin Romeijn^{2,3}, Bart Lynch², Chunhua Men³,
Dionne M Aleman^{4,6} and James F Dempsey^{2,5,7}

¹ Sun Nuclear Corporation, 425-A Pineda Court, Melbourne, FL 32940, USA

² Department of Radiation Oncology, University of Florida, Gainesville, FL 32610-0385, USA

³ Department of Industrial and Systems Engineering, University of Florida, Gainesville, FL 32611-6595, USA

⁴ Department of Mechanical and Industrial Engineering, University of Toronto, Toronto, Ontario, Canada

⁵ ViewRay Incorporated, 101 SE 2nd Place, Suite 201D, Gainesville, FL 32601, USA

E-mail: chrisfox@sunnuclear.com, romeijn@ise.ufl.edu, lynchb@ufl.edu, chhmen@ufl.edu, aleman@mie.utoronto.edu and dempsey@ufl.edu

Received 29 January 2008, in final form 1 April 2008

Published 27 May 2008

Online at stacks.iop.org/PMB/53/3175

Abstract

In this study, we perform a scientific comparative analysis of using ^{60}Co beams in intensity-modulated radiation therapy (IMRT). In particular, we evaluate the treatment plan quality obtained with (i) 6 MV, 18 MV and ^{60}Co IMRT; (ii) different numbers of static multileaf collimator (MLC) delivered ^{60}Co beams and (iii) a helical tomotherapy ^{60}Co beam geometry. We employ a convex fluence map optimization (FMO) model, which allows for the comparison of plan quality between different beam energies and configurations for a given case. A total of 25 clinical patient cases that each contain volumetric CT studies, primary and secondary delineated targets, and contoured structures were studied: 5 head-and-neck (H&N), 5 prostate, 5 central nervous system (CNS), 5 breast and 5 lung cases. The DICOM plan data were anonymized and exported to the University of Florida optimized radiation therapy (UFORT) treatment planning system. The FMO problem was solved for each case for 5–71 equidistant beams as well as a helical geometry for H&N, prostate, CNS and lung cases, and for 3–7 equidistant beams in the upper hemisphere for breast cases, all with 6 MV, 18 MV and ^{60}Co dose models. In all cases, 95% of the target volumes received at least the prescribed dose with clinical sparing criteria for critical organs being met for all structures that were not wholly or

* This work was supported by the National Science Foundation under grant no. DMI-0457394 and the National Cancer Institute under grant no. R01 CA100636.

⁶ The work of this author was supported by The Alliance for Graduate Education and the Professoriate and a Graduate Research Fellowship of the National Science Foundation.

⁷ This author owns stock in and is Chief Science Officer of ViewRay Incorporated and as such may benefit financially as a result of the outcomes of work or research reported in this manuscript.

partially contained within the target volume. Improvements in critical organ sparing were found with an increasing number of equidistant ^{60}Co beams, yet were marginal above 9 beams for H&N, prostate, CNS and lung. Breast cases produced similar plans for 3–7 beams. A helical ^{60}Co beam geometry achieved similar plan quality as static plans with 11 equidistant ^{60}Co beams. Furthermore, 18 MV plans were initially found not to provide the same target coverage as 6 MV and ^{60}Co plans; however, adjusting the trade-offs in the optimization model allowed equivalent target coverage for 18 MV. For plans with comparable target coverage, critical structure sparing was best achieved with 6 MV beams followed closely by ^{60}Co beams, with 18 MV beams requiring significantly increased dose to critical structures. In this paper, we report in detail on a representative set of results from these experiments. The results of the investigation demonstrate the potential for IMRT radiotherapy employing commercially available ^{60}Co sources and a double-focused MLC. Increasing the number of equidistant beams beyond 9 was not observed to significantly improve target coverage or critical organ sparing and static plans were found to produce comparable plans to those obtained using a helical tomotherapy treatment delivery when optimized using the same well-tuned convex FMO model. While previous studies have shown that 18 MV plans are equivalent to 6 MV for prostate IMRT, we found that the 18 MV beams actually required more fluence to provide similar quality target coverage.

1. Introduction

Cobalt teletherapy units and linear accelerator systems (linacs) were introduced nearly simultaneously in the early 1950s and emerged as rival technologies for external beam therapy. The first two ^{60}Co units were installed in Canada in 1951 (Litt 2000) and the first clinical megavoltage (MV) linac was installed in London in 1952 (Bernier *et al* 2004, Thwaites and Tuohy 2006), with the first patient treated with this machine in 1953. The deeply penetrating ionizing photon beams provided by these devices quickly became the mainstay of radiation therapy, allowing for the noninvasive treatment of deep-seated tumors. In particular, both the linac and the cobalt teletherapy unit offered improved skin sparing and penetration over the orthovoltage unit employed until that time. Initially, cobalt teletherapy became the most widespread form of external beam therapy. This was mainly due to the safety, reliability, precision and simplicity of these units, requiring little maintenance and technical expertise to operate, as compared to the technologically intensive linacs. By the late 1960s, there were approximately 1700 external beam devices in the world and approximately 90% of them were cobalt therapy units (Hogstrom and Almond 2006). In the 1970s, major advances were made in the production of electron beams using linacs. Before the discovery and development of intensity-modulated radiation therapy (IMRT), electron beams were demonstrated to provide superior methods for treating cancer of the breast and the head-and-neck (H&N) (Hogstrom and Almond 2006). This, combined with a lack of technical improvements for the cobalt unit (lack of multileaf collimator (or MLC) and digital readout, etc), gave the linac a clinical advantage over the cobalt unit for nearly three decades. By the late 1980s, over 90% of therapy units in the US were linacs, and in the 1990s cobalt therapy units essentially vanished in the US. During this time, great advances were made in beam delivery based on large-scale treatment plan optimization, allowing the clinical application of IMRT using MLCs. With this

advent of MLC-based IMRT, the advantage of combining photon and electron beams vanished as IMRT was performed using only photon beams and could provide excellent treatment plans for cancer of the breast and head-and-neck (Webb 2004). In fact, so did the advantage of high-energy MV photon beams, as it has been demonstrated that IMRT only requires low-energy photon beams to produce high quality treatment plans, even for a deep-seated prostate tumor in exceptionally large patients (Pirzkall *et al* 2002, Sun and Ma 2006).

Although low-energy photon beams have demonstrated efficacy for IMRT, cobalt units have other technical issues when compared with the linac (Laughlin *et al* 1986, Suit 1986). Historically, cobalt therapy systems were noted to suffer from four significant limitations:

- (i) cobalt beams were noted to have a beam edge (or penumbra) that was not as sharp as that of a photon beam that can be produced from a linac;
- (ii) cobalt beams often created high surface doses which could result in skin reactions due to low-energy contamination electrons (scattered from the source and collimators by the photon beam) (Mora *et al* 1999);
- (iii) the most powerful cobalt beams had a lower dose rate than linacs by approximately 60% (with a maximum output of $\sim 250 \text{ cGy min}^{-1}$) and
- (iv) cobalt beams are not as penetrating as higher (10–20) MV beams available on a linac.

These disadvantages, along with the ability of electron beams to produce curative treatment plans for cancers of the breast and head-and-neck (in the pre-IMRT era), resulted in the eventual preference for the linac in the 1970s and 1980s and the eventual demise of cobalt teletherapy as a leading technology in the developed world.

However, cobalt was not without its supporters. In 1986, Laughlin *et al* (1986) published a paper detailing the pros and cons of ^{60}Co and called for a continued push in the technical development of cobalt therapy. That call was reiterated in an editorial by (Suit 1986) in the same journal issue, but went unheeded until now. Recently, development on a novel magnetic resonance image-guided radiation therapy (MRIGRT) device has begun (RenaissanceTM System 1000, ViewRay Incorporated, Gainesville, OH) by the authors of this manuscript. The device is designed to overcome all four of the above-mentioned limitations of cobalt therapy in the following manner:

- (i) the penumbra of a linac with a MLC (which has been measured to be in the range of 4–7 mm depending on manufacturer (Huq *et al* 2002, Kanagaki *et al* 2007, Langen *et al* 2005)) is actually comparable to that of a cobalt unit when a double-focused MLC is employed with a commercially available 2 cm diameter cobalt source (T1000, MDS Nordion; see the results in this paper);
- (ii) the magnetic field of the MRI eliminates contamination electrons and with it the possibility of high surface doses and related skin reactions (Jursinic and Mackie 1996);
- (iii) by utilizing three radiotherapy heads the MRIGRT device provides a competitive dose rate that is higher than a standard linac 2 years after source install and
- (iv) the penetration of a ^{60}Co photon beam is not important with IMRT, which is supported by the results of this manuscript.

Previous work (Laughlin *et al* 1986) has considered the characteristics and merits of beam energies in the range 1–45 MV for conformal photon beams (non-IMRT) and demonstrated that for 3- and 4-beam planning equivalent dose distributions can be achieved with 6, 10 and 18 MV beams and clinical advantages associated with higher energy beams improve little beyond 4 MV. In the case of IMRT, most studies have demonstrated that 6 and 18 MV beams produce equivalent quality treatment plans (Pirzkall *et al* 2002, Sun and Ma 2006, Weiss *et al* 2007), although Madani *et al* (2007) observe some differences depending on the dose

calculation method used. However, comparisons of ^{60}Co and linac treatment planning for IMRT have not been published in the medical physics literature.

Consideration of the IMRT treatment setup must include not only the optimum beam quality but also a decision as to the number of beams and their orientation about the patient. This choice is often left to the discretion of the treatment center and is based on prior knowledge and experience. However, the fundamental question of the optimal number of equidistant beams and beam orientation optimization is still under discussion in the literature, although several studies have shown a sharply declining marginal benefit of using more than 10 equidistant beams for high-energy photon beam IMRT (see, e.g., Bortfeld *et al* (1990), Das *et al* (2003) and Stien *et al* (1997)). Additionally, rotating fan beams have been introduced that utilize a helical treatment pattern by rotating the beam about a 360° gantry and translating the patient couch through it (Beavis 2004, Yang *et al* 1997). This effectively approximates the limit of a large number of coplanar fan beams about the gantry for beam delivery.

The goal of this work is to investigate the use of different numbers of static multileaf collimator (MLC) delivered beams as well as a helical tomotherapy beam geometry in ^{60}Co IMRT. Treatment plans with 5–71 equidistant 6 MV and ^{60}Co beams are compared in terms of target coverage and organ sparing for H&N, prostate, CNS and lung cases, and 3–7 equidistant beams restricted to the upper hemisphere for breast cases. In addition, a helical beam implementation is compared to static field plans for a ^{60}Co beam modality for H&N cases. Finally, 6 MV, 18 MV and ^{60}Co beams were compared for a prostate case.

2. Materials and methods

Five patient cases for each of five typical IMRT treatment sites (H&N, prostate, CNS, breast and lung) were used in our study. H&N and CNS cases contained two targets, referred to as PTV1 and PTV2. For prostate cases, PTV1 contained the prostate gland plus an 8 mm isotropic margin to allow for spatial uncertainties arising from setup errors and physical motions during treatment. Similarly, PTV2 contained the prostate gland and seminal vesicles and an 8 mm isotropic margin. For lung cases, margins were added according to the tumor location. A symmetric margin of 0.5 cm was added to upper lobe tumors while to tumors in the lower lobe a 0.5 cm transversal and 1 cm craniocaudal margin was applied (as in the work by Leter *et al* (2005)). Targets for breast cases were designated as in the work by Hong *et al* (1999), where PTV1 comprised the tumor bed and PTV2 the breast tissue plus nodes with a 1 cm margin in the posterior direction and 2 cm in the superior and inferior. The PTV2 target was extended to the body contour in the anterior direction.

Prescription doses of 73.8 and 54 Gy were assigned to PTV1 and PTV2, respectively, for H&N, prostate and CNS cases. For lung cases, PTV1 and PTV2 were prescribed 70 and 50 Gy, respectively, and in breast cases the prescription doses for PTV1 and PTV2 were 60 and 54 Gy, respectively. Target coverage of 95% volume receiving the prescription dose ($D_{95\%} \geq D_{R_x}$) with the maximum dose limited to $1.1 \times D_{R_x}$ was deemed acceptable. The tolerance doses applied to critical structures are shown in table 1 and are given as maximum tolerance dose allowed or constraints on the dose per volume fraction.

Anonymized DICOM volumetric CT data and delineated targets and structures for all 25 cases were imported into the University of Florida optimized radiation therapy (UFORT) treatment planning decision support system (TPDSS). This treatment planning system has been commissioned for use with 6 MV, 18 MV and ^{60}Co beamlet models from a Varian 2100C/D linac and a Theratronics 1000C cobalt unit (with a commercially available cobalt source (13,000 Ci 2 cm, MDS Nordion) at a 1 m isocenter with a double-focused MLC with its furthest side at 50 cm from the source). These models were fitted to published data and

Table 1. Tolerance criteria for critical structures.

Organ	Criterion	Organ	Criterion
Retina/eye	<45 Gy	Eye lens	<12 Gy
Optic nerve	<50 Gy	Optic chiasm	<55 Gy
Brain stem	<55 Gy	Spinal cord	<45 Gy
Parotid gland	<30 Gy at 50%	Submandibular gland	<30 Gy at 50%
Rectum	<60 Gy at 30%	Bladder	<60 Gy at 30%
Skin	<60 Gy	Mandible	<70 Gy
Individual lung (breast)	<20 Gy at 20%	Total lung (lung)	<40 Gy at 40%
Individual lung (breast)	Mean < 15 Gy	Total lung (lung)	Mean < 15 Gy

validated with radiochromic film of $1 \times 1 \text{ cm}^2$ beamlets formed by the accelerator jaws for 6 and 18 MV and by a Cerrobend block for ^{60}Co . Data were measured using the methods described by Dempsey *et al* (1999), (2000). For the dose calculations, the CT and structure data were mapped to an isotropic grid. Dempsey *et al* (2005) used a Fourier analysis to determine the required resolution for 6 MV beams. In that paper, the 80–20% penumbra for the 6 MV beam was 2.25 mm and the required resolution for 1% accuracy was found to be 2.5 mm. In addition, we found that the 80–20% penumbra for ^{60}Co was 4.5 mm and the required resolution for 1% accuracy was 4–5 mm. Hence, in order to ensure that all relevant information in the dose distribution was captured we employed voxels of size $2.5 \times 2.5 \times 2.5 \text{ mm}^3$ for 6 and 18 MV and $4 \times 4 \times 4 \text{ mm}^3$ for ^{60}Co . The UFORT TPDSS uses a point-in-polygon technique to associate structures with voxels in the grid and a combination of stereographic projection and three-dimensional ray-tracing is used to determine density scaled depths (see Fox *et al* (2006)) to account for heterogeneities and establish those voxels intersected by each beamlet that traverses the target volume. Relative intensities at intersected voxels from each beamlet are determined, yielding dose deposition coefficients D_{ijs} , representing the dose deposited per unit intensity from beamlet i to voxel j contained within structure s . These coefficients are then input into a fluence map optimization (FMO) model. As is standard in treatment plan optimization models, the dose d_{js} deposited in a voxel j contained within structure s is the result of the superposition of the intensity-weighted beamlet dose depositions, formally given by the linear expression

$$d_{js} = \sum_i D_{ijs} x_i$$

where x_i is the (nonnegative) intensity or weighting factor associated with beamlet i . Our FMO model (see, e.g., Romeijn *et al* (2003), (2004) and Tsien *et al* (2003)) is an analytic nonlinear convex model that employs voxel-based penalty functions. In particular, the objective function is formulated as

$$f = \sum_s \sum_j (\alpha_s^+ \max\{d_{js} - t_s^+, 0\}^{n_s^+} + \alpha_s^- \max\{t_s^- - d_{js}, 0\}^{n_s^-})$$

where, for each structure s , α_s^+ and α_s^- are the importance weights assigned to overdosing and underdosing, t_s^+ and t_s^- are the thresholds associated with overdosing and underdosing, and n_s^+ and n_s^- are powers that ensure that the objective function value f is adversely and disproportionately affected as the dose moves away from the threshold values. Typically, both overdosing and underdosing penalties are included for targets while only overdosing penalties are included for critical structures. Targets are assigned the highest importance in the FMO model to ensure that the target coverage criteria are met, which is particularly important when overlap of targets and critical structures occurs. Similar tuning parameters were used for each

case with minor adjustments to improve target coverage and structure sparing as required. The optimal intensities of the available beamlets are then determined by optimizing the problem to provide a fluence map that gives a high-quality dose distribution satisfying the desired clinical criteria as described below.

FMO problems were solved to obtain treatment plans for H&N, prostate, CNS and lung cases using 5, 7, 9, 11, 17, 35 and 71 equidistant beam angles. Breast cases were restricted to a 180° arc above the breast to remove beamlets that enter the posterior to reach the tumor, and FMO problems were solved for 3, 5 and 7 equidistant beams. Plan quality was assessed via dose–volume histogram (DVH) and spatial dose distribution evaluation. A comparison of the plan quality between the 6 MV, 18 MV and ⁶⁰Co was performed and the impact of varying the number of equidistant coplanar beams on target coverage and critical structure sparing investigated. A helical scanning treatment beam was implemented in the UFORT TPDSS with the 6 MV and ⁶⁰Co beam models. A maximum collimator opening of 40 × 2 cm² was allowed with bixel size of 1 × 1 cm² and pitch 0.5. The start and end point of the helices was established from the limits of targets in the cranium–caudal orientation with an additional margin of 1 cm.

The convex FMO model was solved by employing a projected gradient algorithm with Armijo line search (Kelley 1987). This yields a fast method that produces excellent target coverage and organ sparing. Our implementation of the projected gradient algorithm proceeds as follows. In a given iteration, k , with current solution $x^{(k)}$, the next solution is given by

$$x^{(k+1)} = \max\{x^{(k)} - \lambda^* \nabla f_k, 0\}$$

where ∇f_k is the gradient of f evaluated at $x^{(k)}$ and λ^* is found by a search along the projected path $\max\{x^{(k)} - \lambda \nabla f_k, 0\}$ parameterized by the nonnegative step length λ . The search direction, being the negative of the gradient of f at the current solution, is a descent direction so that the result of the line search is a solution with a lower (i.e., improved) objective function value (see figure 1). The performance of the algorithm depends greatly on the step length. If the step length is too short the convergence of the algorithm will require a large number of iterations and will therefore be slow. On the other hand, if the step size is too large the optimal solution may be overshoot, producing an insufficient reduction in the objective function in each step, again preventing fast convergence. In each iteration, a good step size can be obtained by (i) trying several test candidate values for λ and (ii) choosing the one that provides the largest improvement in objective function value. The Armijo line search method determines the step size by iteratively stepping backwards from a maximum step size along the search direction until a solution is found that attains a reduction in objective function value. Finally, the leaf-sequencing algorithm of Kamath *et al* (2003) was applied to the fluence maps obtained by the FMO to determine the number of MLC-shaped apertures required to successfully deliver the fluence map.

3. Results and discussion

3.1. ⁶⁰Co beamlet analysis

Figure 2 shows a profile of the radiochromic film measurement of a 2 × 2 cm² ⁶⁰Co beamlet measured on a Theratronics 1000C Cobalt unit at 0.5 cm depth in a 30 × 30 cm² solid water phantom at 100 cm source to surface distance using a divergent 10 cm thick Cerrobend collimator with its distal end at 50 cm from the source. The beamlet was measured on the central axis; however, the cobalt source has a very even energy spectrum and no flattening filter so that the off-axis beamlets are very similar. An 80–20% penumbra distance of

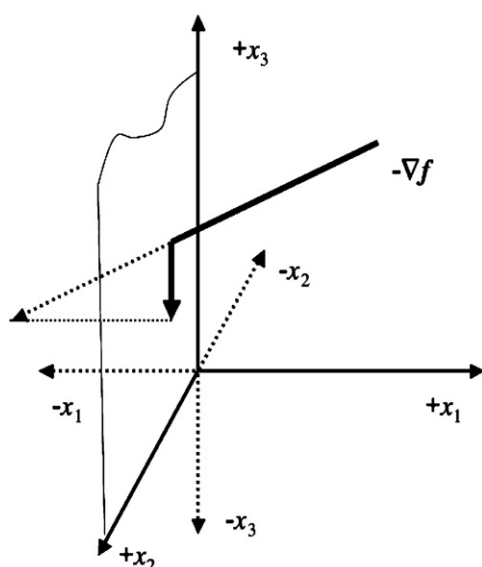


Figure 1. Example of a projected gradient step.

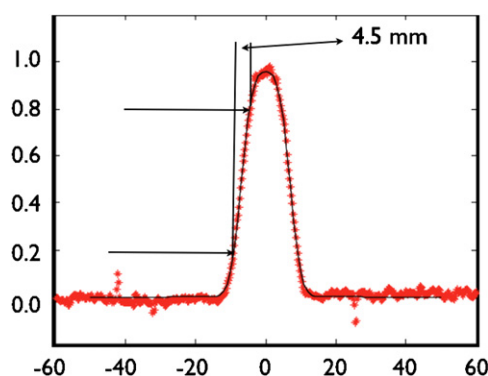


Figure 2. A $2 \times 2 \text{ cm}^2$ ^{60}Co beamlet measured on a Theratronics 1000 C Cobalt unit.

4.5 mm was observed. Note that our results are consistent with the measured penumbra of cobalt sources reported in Adams and Warrington (2008), Poffenbarger and Podgorsak (1998), Raja Singh *et al* (2000) and Warrington and Adams (2002).

3.2. Comparative analysis of 6 MV and ^{60}Co beam IMRT plans

Figures 3(a), (c), (e), (g) and (i) show the DVHs for two 7-beam IMRT plans obtained for a typical case from each of the five sites studied (H&N, prostate, CNS, lung and breast), where the other cases showed comparable behavior. The solid lines represent plans for a 6 MV dose model while the dashed lines represent plans for a ^{60}Co dose model.

For the H&N case (figure 3(a)), with both 6 MV and ^{60}Co a treatment plan that achieves the required dose coverage of $D_{95\%} > D_{R_x}$ for the PTV1 and PTV2 was obtained while maintaining the submandibular and parotid glands within the criteria set in table 1. Target coverage is almost identical for both beam qualities. The four glands at the tolerance limits show minor variations between the two beams. The 6 MV beams produced slightly better

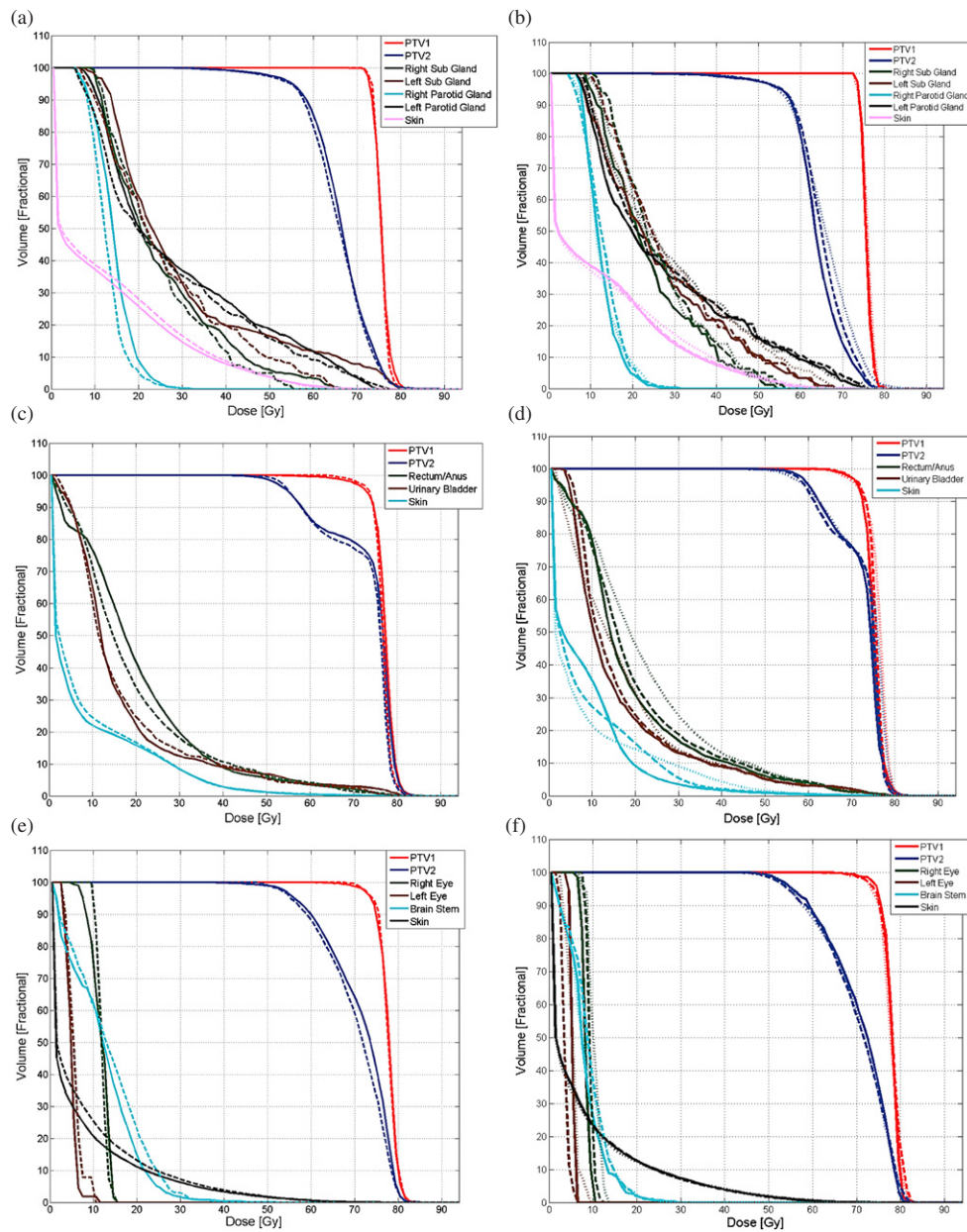


Figure 3. DVHs for typical clinical cases. Parts (a), (c) and (e) show a comparison of 6 MV (solid) and ^{60}Co (dashed) for 7 equidistant beams for H&N, prostate and CNS cases. Parts (b), (d) and (f) compare 5 (dotted), 9 (dashed) and 71 (solid) equidistant beams for the ^{60}Co dose model for H&N, prostate and CNS cases. Parts (g) and (i) show a comparison of 6 MV (solid) and ^{60}Co (dashed) for 7 equidistant beams for a lung case and 7 equidistant beams in the upper hemisphere for a breast case. Part (h) compares 5 (dotted), 9 (dashed) and 71 (solid) equidistant beams for the ^{60}Co dose model for a lung case, and part (j) compares 3 (dashed) and 5 (solid) equidistant beams in the upper hemisphere for the ^{60}Co dose model for a breast case.

sparing for left parotid and submandibular glands, at the sparing criterion condition, while ^{60}Co showed improved results for the right submandibular gland. These differences were not

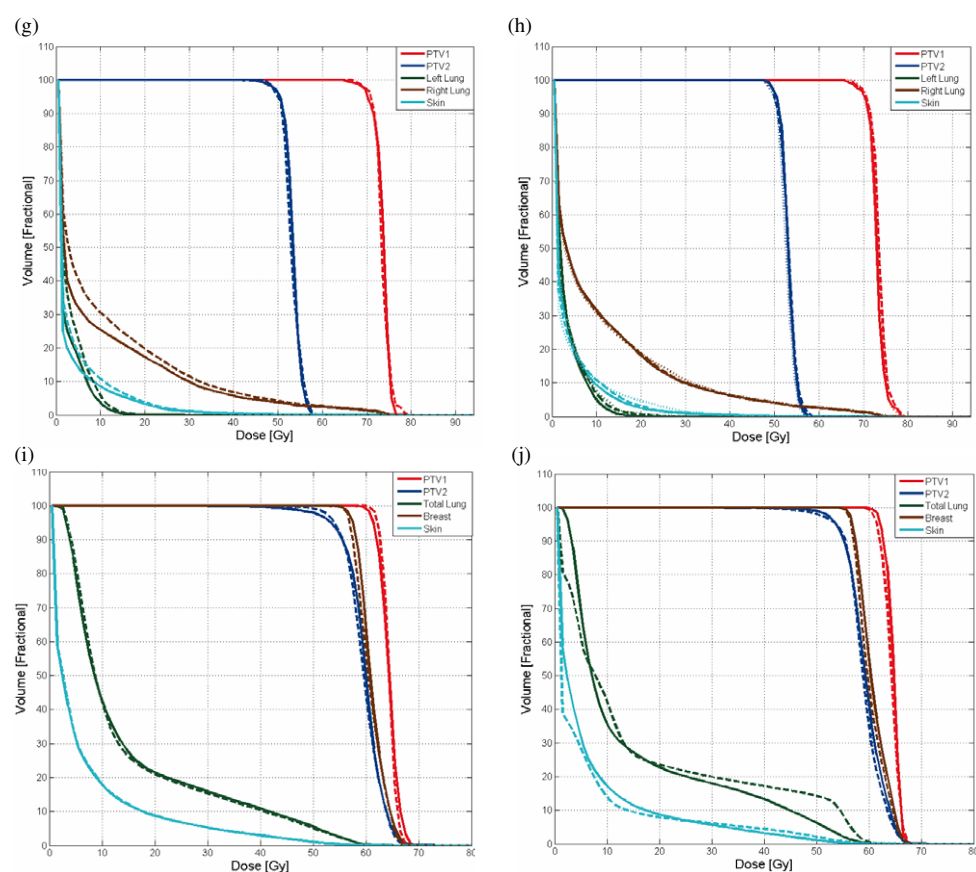


Figure 3. (Continued.)

deemed clinically significant and can be attributed to differences in the trade-offs made by the FMO model. The DVH above 30 Gy is observed to decrease more rapidly for ^{60}Co . At 50 Gy, the DVH for ^{60}Co is 3–4% lower compared to 6 MV and is most likely the result of the FMO model's ability to take advantage of the reduced exit dose associated with the lower penetrability of the ^{60}Co beam.

For the prostate case (figure 3(c)), equivalent target coverage was observed with both 6 MV and ^{60}Co for 7-beam plans. Below 30 Gy, the rectum is observed to receive ~ 2 –3 Gy less per volume than with 6 MV with the urinary bladder receiving approximately the same dose for each beam quality below 30 Gy. At the tolerance limits ($< 30\%$ at 60 Gy), the dose from both modalities is the same for the urinary bladder and rectum. The lower maximum dose observed in the bladder and rectum using ^{60}Co results from the higher attenuation of the beam compared to 6 MV.

CNS cases are the simplest to solve, primarily due to the lack of proximity of the targets to critical structures. Figure 3(e) shows that the required target coverage of $D_{95\%} > D_{R_x}$ is achieved for both cases with only minor variations for 7-beam plans.

Figures 3(g) and (i) show a similar pattern for the lung and breast cases, respectively. In addition, for the breast case the mean dose to total lung was virtually identical at about 11 Gy for both 6 MV and ^{60}Co , while for the lung case marginally lower mean dose to both lungs was observed for 6 MV than for ^{60}Co (about 10 versus 11 Gy for right lung and about 2 versus

2.5 Gy for left lung), but all observed mean lung doses were well below the tolerance limit. In summary, in both cases plan quality is similar between the 6 MV and ^{60}Co modalities with 7 beams.

3.3. Comparative analysis of varying the number of beams

Figures 3(b), (d), (f), (h) and (j) show the DVHs for IMRT plans obtained for a typical case from each of the five sites with different numbers of equidistant ^{60}Co beams; the other cases exhibited similar behavior. In particular, in figures 3(b), (d), (f) and (h) (H&N, prostate, CNS and lung, respectively) the dotted lines correspond to 5-beam plans, the dashed lines to 9-beam plans and the solid lines to 71-beam plans, while in figure 3(j) (breast) the dashed lines correspond to a 3-beam plan while the solid lines correspond to a 5-beam plan.

For the H&N case (figure 3(b)), good target coverage is observed with as few as five equidistant coplanar beams while the sparing criteria given in table 1 are maintained. The threshold of 95% target volume receiving the prescription dose is attained for the PTV1 and PTV2 with 5, 9 and 71 beams. The PTV1 coverage is the same for each set of equidistant beams. However, the hot spot of the PTV2 at 20% volume improves by $\sim 5\%$ between the 5- and 9-beam plans. Further increasing the number of beams shows only minor improvements in the hot spot of the PTV2. Gland coverage shows a similar trend at 30 Gy with a reduction in the dose per volume of 3–10% when the number of beams is increased from 5 to 9 beams. Increasing the number of beams up to 71 shows little change as compared to 9 beams. Figure 4 illustrates the dose distributions obtained for 7 and 71 beams from the 6 MV and ^{60}Co dose models. Only minor variations are observed between the two treatment modalities, and similar dose distributions for targets and critical structures were observed for 7 and 71 beams.

As for the H&N case, the prostate plans demonstrate similar coverage of the PTV1 and PTV2 using 5, 9 and 71 beams (figure 3(d)). The dose to the urinary bladder and rectum is below accepted tolerances of 30% volume to receive less than 60 Gy for all three beam numbers. Below 40 Gy a marked increase in dose to critical structures is observed when the number of beams is decreased. The 5-beam plan results in ~ 5 Gy higher dose to 30% of the rectum volume as compared to the 9- and 71-beam plans, for which the corresponding dose is 20 Gy. The dose distribution of the skin varies considerably with changing number of beams. The 71-beam plan gives a lower dose to a larger percentage of the skin than the 5-beam plan: with the former plan 35% receives in excess of 10 Gy and about 3% in excess of 30 Gy, while with the latter plan only 20% of the skin receives in excess of 10 Gy and about 9% in excess of 30 Gy. This is likely the result of spreading the incident dose over a larger surface area with more beams. Figure 5 illustrates the dose distributions obtained for 7 and 71 beams from the 6 MV and ^{60}Co dose models. As for the H&N case, the variations observed between both the treatment modalities are small and clinically comparable dose distributions for targets and critical structures are obtained with 7 and 71 beams.

For both the CNS and the lung cases (figures 3(f) and (h)) only marginal improvements are observed when the number of beams increases from 5 to 9. For the lung case, the mean dose to either lung is virtually independent of the number of beams at 10–11 Gy for the right lung and <3 Gy for the left lung. Overall, all criteria are well within the tolerances and little further improvements are seen in the 71-beam plans over the 9-beam plans.

Finally, figure 3(j) shows the DVHs for 3-beam and a 5-beam ^{60}Co breast plan. (Note that beams for breast cases are restricted to a 180° arc above the breast tissue.) Comparing these DVHs with figure 3(i), which shows a 7-beam plan, the total lung dose is observed to fall off faster as the number of beams increases. In each case, the maximum dose received to

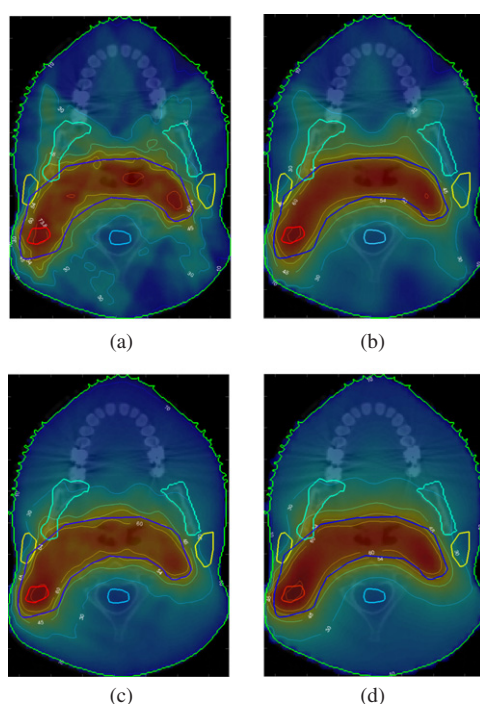


Figure 4. Deliverable IMRT axial isodose distributions for a H&N IMRT case. Parts (a) and (b) show 7-beam dose distributions for 6 MV and ^{60}Co , respectively. Parts (c) and (d) are 71-beam dose distributions for 6 MV and ^{60}Co , respectively. Shown are PTV1 (red) and PTV2 (dark blue) as well as the parotid glands (yellow), mandible (light green), spinal cord (light blue) and skin (bright green). Isodose curves are shown for 73.8, 60, 54, 45, 30 and 10 Gy.

the total lung is 60 Gy, the mean dose to lung is below the threshold at about 11–13 Gy, and the tolerance limit of no more than 20% lung volume receiving in excess of 40 Gy is also met.

3.4. Comparative analysis of 6 MV, 18 MV and ^{60}Co IMRT for prostate

Figure 6(a) shows an 18 MV dose model applied to a prostate case compared to 6 MV and ^{60}Co plans for the same case. The 18 MV beam model plan achieves the sparing criteria given in table 1 for the urinary bladder and rectum and the coverage of PTV1 and PTV2 attains the 95% volume receiving the prescription dose. However, the falloff in both the PTV2 and PTV1 is less sharp with the 18 MV beam and additional tuning of the objective function parameters produced little improvement and showed a marked increase of the rectum and urinary dose per volume around the 40% mark. The urinary bladder receives a consistently higher dose per volume with the 18 MV model, reaching a maximum of 20% volume having 20 Gy above that observed with the 6 MV case. This was also the case for the skin and parts of the rectum.

3.5. Comparative analysis of helical and static ^{60}Co for H&N

Figure 6(b) shows a H&N plan obtained using a helical ^{60}Co beam scanning pattern for the treatment delivery (dotted lines) as well as a plan for the same patient obtained with 11 static equidistant ^{60}Co beams (solid lines). Target coverage and critical structure sparing criteria are maintained for both plans. The target DVHs are almost identical, with the 11-beam static

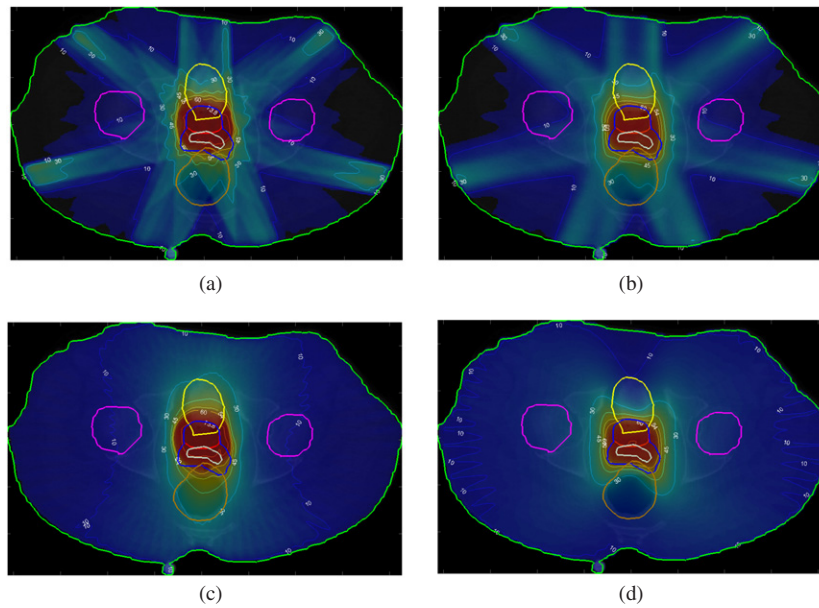


Figure 5. Deliverable IMRT axial isodose distributions for a prostate IMRT case. Parts (a) and (b) show 7-beam dose distributions for 6 MV and ^{60}Co , respectively. Parts (c) and (d) are 71-beam dose distributions for 6 MV and ^{60}Co , respectively. Shown are PTV1 (red) and PTV2 (dark blue) as well as bladder (yellow), rectum (brown), femoral heads (purple) and skin (bright green). Isodose curves are shown for 73.8, 60, 54, 45, 30 and 10 Gy.

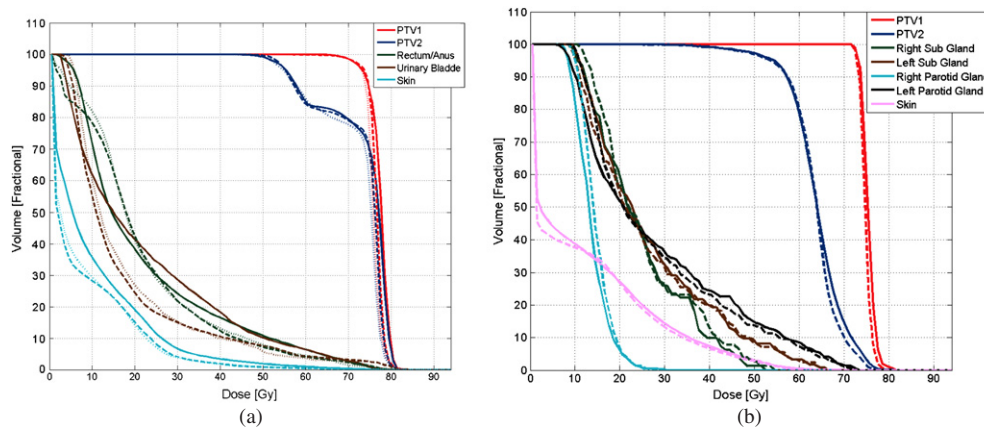


Figure 6. (a) Comparison of an 18 MV (solid), 6 MV (dashed) and ^{60}Co (dotted) dose model for a static 11-beam prostate plan. (b) Comparison of a static 11-beam ^{60}Co (solid line) plan to that of a helical ^{60}Co (dotted line) plan for a H&N case.

plan showing a maximum divergence at the 15% volume level of 2 Gy for PTV2 and 1 Gy for PTV1, while the critical structure DVHs are virtually indistinguishable from one another.

3.6. Number of apertures

Finally, the leaf-sequencing algorithm was applied to the 25 cases investigated. To illustrate these results, table 2 shows, for a single case for each of the five sites and for both 6 MV and

Table 2. Number of apertures required for typical cases.

Number of beams	H&N		Prostate		CNS		Lung		Breast	
	6 MV	^{60}Co	6 MV	^{60}Co	6 MV	^{60}Co	6 MV	^{60}Co	6 MV	^{60}Co
3									89	89
5	164	150	130	135	108	107	104	107	157	137
7	226	224	167	209	150	151	257	276	192	180
9	283	316	219	238	188	195	328	353		
11	354	374	282	283	233	237	409	432		
17	504	537	397	480	346	358	630	662		
35	1014	1178	890	965	788	770	1249	1385		
71	2330	2455	1743	1976	1623	1569	2561	2969		

^{60}Co beams, the number of apertures required to deliver the fluence map obtained from the FMO using the leaf-sequencing algorithm. The number of apertures varied from ~ 90 for a 3-beam breast plan up to ~ 3000 for a 71-beam lung plan. For typical 7-beam plans, the H&N cases required on the order of 225 apertures, compared to approximately 200 for prostate, 150 for CNS and 275 for lung. In general, the number of apertures required increased linearly with the number of beams for all sites and for both beam qualities. No trend was observed between the target volume and aperture number. Finally, fluence maps that contain a larger number of gradient changes across the profile generally require a larger number of apertures to successfully deliver the FMO fluence map using a MLC.

4. Conclusions

The data presented demonstrates that excellent plan quality for IMRT using inverse treatment planning can be achieved with low numbers of equidistant beams, with little gain from extending beam numbers beyond 9 beams in terms of target coverage and critical organ sparing. We also demonstrate the feasibility of employing commercial ^{60}Co sources with a divergent MLC for IMRT and show that nearly identical plans can be achieved when compared to 6 MV IMRT. We therefore conclude that the common assumption that the ^{60}Co penumbra is inferior to linac penumbra for MLC-based IMRT is not supported by the literature (see, e.g., Huq *et al* (2002), Kanagaki *et al* (2007), Langen *et al* (2005) or the findings of this study.

References

- Adams E J and Warrington A P 2008 A comparison between cobalt and linear accelerator-based treatment plans for conformal and intensity-modulated radiotherapy *Br. J. Radiol.* **81** 304–10
- Beavis A W 2004 Is tomotherapy the future of IMRT? *Br. J. Radiol.* **77** 285–95
- Bernier J, Hall E J and Giaccia A 2004 Radiation oncology: a century of achievements *Nature Rev. Cancer* **4** 737–47
- Bortfeld T, Burkelbach J, Boesecke R and Schlegel W 1990 Methods of image reconstruction from projections applied to conformal radiotherapy *Phys. Med. Biol.* **25** 435–43
- Das S, Cullip T, Tracton G, Chang A, Marks L, Anscher M and Rosenman J 2003 Beam orientation selection for intensity-modulated radiation therapy based on target equivalent uniform dose maximization *Int. J. Radiat. Oncol. Biol. Phys.* **55** 215–24
- Dempsey J F, Low D A, Kirov A S and Williamson J F 1999 Quantitative optical densitometry with scanning-laser film digitizers *Med. Phys.* **26** 1721–31
- Dempsey J F, Low D A, Mutic S, Markman J, Kirov A S, Nussbaum G H and Williamson J F 2000 Validation of a precision radiochromic film dosimetry system for quantitative two-dimensional imaging of acute exposure dose distributions *Med. Phys.* **27** 2462–75

- Dempsey J F, Romeijn H E, Li J G, Low D A and Palta J R 2005 A Fourier analysis of the dose grid resolution required for accurate IMRT fluence map optimization *Med. Phys.* **32** 380–8
- Fox C, Romeijn H E and Dempsey J F 2006 Fast voxel and polygon ray-tracing algorithms in IMRT treatment planning *Med. Phys.* **33** 1364–71
- Hogstrom K R and Almond P R 2006 Review of electron beam therapy physics *Phys. Med. Biol.* **51** R455–89
- Hong L, Hunt M, Chui C, Spirou S, Forester K, Lee H, Yahalom J, Kutcher G J and McCormick B 1999 Intensity-modulated tangential beam irradiation of the intact breast *Int. J. Radiat. Oncol. Biol. Phys.* **44** 1155–64
- Huq M S, Das I J, Steinberg T and Galvin J M 2002 A dosimetric comparison of various multileaf collimators *Phys. Med. Biol.* **47** N159–70
- Jursinic P A and Mackie T R 1996 Characteristics of secondary electrons produced by 6, 10 and 24 MV x-ray beams *Phys. Med. Biol.* **41** 1499–509
- Kamath S, Sahni S, Li J, Palta J and Ranka S 2003 Leaf sequencing algorithms for segmented multileaf collimation *Phys. Med. Biol.* **48** 307–24
- Kanagaki B, Read P W, Molloy J A, Larner J M and Sheng K 2007 A motion phantom study on helical tomotherapy: the dosimetric impacts of delivery technique and motion *Phys. Med. Biol.* **52** 243–55
- Kelley C T 1987 *Iterative Methods in Optimization* (Philadelphia: SIAM)
- Langen K M, Meeks S L, Poole D O, Wagner T H, Willoughby T R, Zeidan O A, Kupelian P A, Ruchala K J and Oliveira G H 2005 Evaluation of a diode array for QA measurements on a helical tomotherapy unit *Med. Phys.* **32** 3424–30
- Laughlin J S, Mohan R and Kutcher G J 1986 Choice of optimum megavoltage for accelerators for photon beam treatment *Int. J. Radiat. Oncol. Biol. Phys.* **12** 1551–7
- Leter E M, Cademartiri F, Levendag P C, Flohr T, Stam H and Nowak P J 2005 Four-dimensional multi slice computed tomography for determination of respiratory lung tumor motion in conformal radiotherapy *Int. J. Radiat. Oncol. Biol. Phys.* **62** 888–92
- Litt P 2000 *Isotopes and Innovation: MDS Nordion's First Fifty Years, 1946–1996* (Montreal: McGill-Queens University Press)
- Madani I, Vanderstraeten B, Bral S, Coghe M, De Gersem W, De Wagter C, Thierens H and De Neve W 2007 Comparison of 6 MV and 18 MV photons for IMRT treatment of lung cancer *Radiother. Oncol.* **82** 63–9
- Mora G M, Maio A and Rogers D W O 1999 Monte Carlo simulation of a typical 60 Co therapy source *Med. Phys.* **26** 2494–502
- Pirzkall A, Carol M P, Pickett B, Xia P, Roach M III and Verhey L J 2002 The effect of beam energy and number of fields on photon-based IMRT for deep-seated targets *Int. J. Radiat. Oncol. Biol. Phys.* **53** 434–42
- Poffenbarger B A and Podgorsak E B 1998 Viability of an isocentric cobalt-60 teletherapy unit for stereotactic radiosurgery *Med. Phys.* **25** 1935–43
- Raja Singh R, Ravindran P, Nizin P S and Ayyangar K 2000 Dosimetric study of the narrow beams of ⁶⁰Co teletherapy unit for stereotactic radiosurgery *Med. Dosim.* **25** 163–9
- Romeijn H E, Ahuja R K, Dempsey J F, Kumar A and Li J G 2003 A novel linear programming approach to fluence map optimization for intensity modulated radiation therapy treatment planning *Phys. Med. Biol.* **48** 3521–42
- Romeijn H E, Dempsey J F and Li J G 2004 A unifying framework for multi-criteria fluence map optimization models *Phys. Med. Biol.* **49** 1991–2013
- Stien J, Mohan R, Wang X-H, Bortfeld T, Wu Q, Preiser K, Ling C C and Schlegel W 1997 Number and orientations of beams in intensity-modulated radiation treatments *Med. Phys.* **24** 149–60
- Suit H 1986 What's the optimum choice? *Int. J. Radiat. Oncol. Biol. Phys.* **12** 1711–2
- Sun M and Ma L 2006 Treatments of exceptionally large prostate cancer patients with low-energy intensity-modulated photons *J. Appl. Clin. Med. Phys.* **7** 43–9
- Thwaites D I and Tuohy J B 2006 Back to the future: the history and development of the clinical linear accelerator *Phys. Med. Biol.* **51** R343–62
- Tsien C, Eisbruch A, McShan D, Kessler M, Marsh R and Fraass B 2003 Intensity-modulated radiation therapy (IMRT) for locally advanced paranasal sinus tumors: incorporating clinical decisions in the optimization process *Int. J. Radiat. Oncol. Biol. Phys.* **55** 776–84
- Warrington A P and Adams E J 2002 Cobalt 60 teletherapy for cancer: a revived treatment modality for the 21st century *IEE Seminar on Appropriate Medical Technology for Developing Countries*
- Webb S 2004 *Contemporary IMRT: Developing Physics and Clinical Implementation* (Madison, WI: Advanced Medical Publishing)
- Weiss E, Siebers J V and Keall P J 2007 An analysis of 6-MV versus 18-MV photon energy plans for intensity-modulated radiation therapy (IMRT) of lung cancer *Radiother. Oncol.* **82** 55–62
- Yang J, Mackie T R, Reckwerdt P, Deasy J O and Thomadsen B R 1997 An investigation of tomotherapy beam delivery *Med. Phys.* **24** 425–36